High Regularity Porous Oxophilic Metal Films on Pt as Model Bifunctional Catalysts for Methanol Oxidation

Fang Liu,[†] Qingfeng Yan,[†] Wei Jiang Zhou,[†] Xiu Song Zhao,[†] and Jim Yang Lee*[,†,‡]

Chemical & Biomolecular Engineering, National University of Singapore, 10 Kent Ridge Crescent, Singapore 119260, and Singapore-MIT Alliance, 4 Engineering Drive 3, National University of Singapore, Singapore 117576

Received March 13, 2006. Revised Manuscript Received July 10, 2006

Macroporous Ru, Os, Re, RuOs, and RuRe films were deposited on the Pt substrate by a hard template method in which electrodeposition of the oxophilic metal was confined to the interstices formed by annealed closely packed uniform polystyrene spheres self-assembled on the Pt substrate. X-ray diffractometry indicated that co-deposited RuOs and RuRe adopted the ruthenium's hcp (hexagonal close-packed) structure with some negative shifts in the Bragg angles. X-ray photoelectron spectroscopy detected the following major oxidation states on the metal surface: Pt^0 on Pt; Ru^0 on Ru, RuOs, and RuRe; Os^0 on Os and RuOs; and Re^{VII} on Re and RuRe. Both CO stripping voltammetry and chronoamperometric measurements showed that the Pt−RuOs pair sites were most active for sustained CO oxidation, followed by the Pt−RuRe, Pt−Ru, and Pt−Os pair sites, in that order. The trend is explained in terms of the strength of OH adsorption on the oxophilic metals and the contributions of OH_{ad} to the overall methanol oxidation reaction. The use of regular structured porous films on the Pt substrate with distinct Pt−oxophilic metal(s) interfaces removes many of the ambiguities in assigning the observed activity difference to the effects of different Pt−oxophilic metal pair sites.

1. Introduction

Platinum is undoubtedly the most recognized metal for activating methanol in acidic solutions. Platinum is, however, ineffective for the room temperature electrooxidation of methanol because it lacks an efficient mechanism to remove the tenaciously held CO-like reaction intermediates at low temperatures.[1] According to the theory of bifunctional catalysis,[2] an oxophilic metal in which water dissociation is promoted under conditions of methanol activation on Pt can be used in conjunction with Pt to convert the CO-like intermediates into CO_2. Hence, metals such as Ru,[3−11] Re,[4,12] and Os[5−8,13−15] have been used to alloy with Pt to form binary[3,4,6,13−15] or ternary catalyst systems.[5,7,8] It is believed that pair sites consisting of Pt and neighboring oxophilic metal atoms are the active sites for methanol electrooxidation. The activity difference between different Pt−oxophilic metal(s) pair sites is, therefore, of fundamental interest and application relevance (for the development of direct methanol fuel cells, or DMFCs). However, common methods of preparation of multicomponent catalysts including co-impregnation,[9] coprecipitaion,[10] and microemulsion syntheses[11] do not provide sufficient control over particle size and catalyst composition to allow for an unambiguous determination of the intrinsic properties of the pair sites. In our previous work,[16] electrodeposited multi-segment nanorods with customizable and reproducible interfaces were used to demonstrate the existence of bimetallic pair sites and to compare their intrinsic differences. This work presents another method of fabrication of the pair sites which is more able to filter out the influence of the Pt-only sites, to validate the findings of the first work, and to conduct comparisons of additional Pt−oxophilic metal pair sites.

The model catalysts in this work relied on three-dimensionally ordered macroporous films to deliver a new periodic structure. Three-dimensionally ordered macroporous films can be fabricated using closely packed colloidal particles as the template to build an inverse structure of the

* Corresponding author. E-mail: cheleejy@nus.edu.sg. Fax: 65-67791936. Tel.: 65-68742899.
[†] Chemical & Biomolecular Engineering.
[‡] Singapore-MIT Alliance.

(1) Antolini, E. *Mater. Chem. Phys.* **2003**, *78*, 563.
(2) Watanabe, M.; Motoo, S. *J. Electroanal. Chem.* **1975**, *60*, 267.
(3) Iwasita, T.; Hoster, H.; John-Anacker, A.; Lin, W. F.; Vielstich, W. *Langmuir* **2000**, *16*, 522.
(4) Beden, B.; Kadirgan, F.; Lamy, C.; Leger, J. M. *J. Electroanal. Chem.* **1981**, *127*, 75.
(5) Gurau, B.; Viswanathan, R.; Liu, R.; Lafrenz, T.; Ley, K. L.; Smotkin, E. S.; Reddington, E.; Sapienza, A.; Chan, B. C.; Mallouk, T. E.; Sarangapani, S. *J. Phys. Chem. B* **1998**, *102*, 9997.
(6) Crown, A.; Moraes, I. R.; Wieckowski, A. *J. Electroanal. Chem.* **2001**, *500*, 333.
(7) Kessler, T.; Luna, A. M. C. *J. Solid State Electrochem.* **2003**, *7*, 593.
(8) Ley, K. L.; Liu, R.; Pu, C.; Fan, Q.; Leyarovska, N.; Segre, C.; Smotkin, E. S. *J. Electrochem. Soc.* **1997**, *144*, 1543.
(9) Giroir-Fendler, A.; Richard, D.; Gallezot, P. *Faraday Discuss.* **1991**, *92*, 69.
(10) Watanabe, M.; Uchida, M.; Motoo, S. *J. Electroanal. Chem.* **1987**, *229*, 395.
(11) Zhang, X.; Chan, K.-Y. *Chem. Mater.* **2003**, *15*, 451.
(12) Anderson, A. D.; Delug, G. A.; Moore, J. T.; Vergne, M. J.; Hercules, D. M.; Kenik, E. A.; Lukehart, C. M. *J. Nanosci. Nanotechnol.* **2004**, *4*, 809.
(13) Moore, J. T.; Chu, D.; Jiang, R.; Deluga, G. A.; Lukehart, C. M. *Chem. Mater.* **2003**, *15*.
(14) Zhu, Y.; Cabrera, C. R. *Electrochem. Solid State Lett.* **2001**, *4*, A45.
(15) Huang, J.; Yang, H.; Huang, Q.; Tang, Y.; Lu, T.; Akins, D. L. *J. Electrochem. Soc.* **2004**, *151*, A1810.
(16) Liu, F.; Lee, J. Y.; Zhou, W. J. *Small* **2006**, *2*, 121.

10.1021/cm0606023 CCC: $33.50
Published on Web 08/12/2006

Table 1. Compositions of Plating Solutions and Conditions for Electrodeposition of Porous Ru, Os, Re, RuOs, and RuRe Films on the Pt Substrate

	Ru plating solution	Os plating solution	Re plating solution	RuOs plating solution	RuRe plating solution
$Ru(NO)Cl_3$	1.75 g L^{-1}			1.31 g L^{-1}	1.31 g L^{-1}
NH_2SO_3H	5 g L^{-1}			3.74 g L^{-1}	3.74 g L^{-1}
$KReO_4$			5.786 g L^{-1}		0.579 g L^{-1}
H_2SO_4			10 g L^{-1}		1.0 g L^{-1}
K_2OsCl_6		2.5 g L^{-1}		0.417 g L^{-1}	
$KHSO_4$		15 g L^{-1}		2.5 g L^{-1}	
SDS	2.884 g L^{-1}	2.884 g L^{-1}	2.884 g L^{-1}	2.884 g L^{-1}	2.884 g L^{-1}
temperature	55 °C	70 °C	70 °C	70 °C	70 °C
number of cycles[a]	60 000	96 000	96 000	64 000	64 000

[a] For the pulse electrodeposition of Ru, the pulse used was 0 V for 0.0005 s and −0.7 V for 0.0005 s; for the pulse electrodeposition of other metals, the pulse used was 0 V for 0.0005 s and −0.7 V for 0.0005 s.

target material. Many techniques can be used to fill the interstices of the template with the target material; among them electrodepostion is best known for its capability of large area replication and complete in-filling of thick high-dielectric colloidal crystals with conductive materials (e.g., metals,[17−21] polymers,[22−24] and semiconductors[22,25−28]). In this study macroporous films of oxophilic metals on Pt substrates were patterned by electrodeposition of the oxophilic metals (Ru, Re, Os, RuRe, and RuOs) into the interstices of closely packed polystyrene (PS) spheres self-assembled on the Pt substrate. The films contained distinct and quantifiable interfaces between Pt and the oxophilic metal, thereby enabling a direct comparison of the activities of different pair sites. The primary advantage of macroporous films over multi-segment nanorods is the larger bimetallic pair site to Pt site ratio, which increases the contributions from the pair sites and decreases the influence from the Pt sites. The observed activity difference can then be associated with the composition of the pair sites with increased confidence. The pair sites that were evaluated by this new model structure are Pt−Ru, Pt−Re, Pt−Os, Pt−RuRe, and Pt−RuOs, without interference from factors such as particle size, surface enrichment effect, and inhomogeneity in catalyst composition.

2. Experimental Section

2.1. Materials. Ruthenium(III) nitrosyl chloride hydrate, potassium perrhenate, and potassium hexachloroosmate(IV) from Aldrich; potassium hydrogen sulfate and sodium dodecyl sulfate (SDS) from Sigma-Aldrich; sulfuric acid (95−97%) and perchloric acid from Merck; methanol and tetrahydrofuran from Fisher; sulfamic acid from Avocado Research Chemicals; and 30% hydrogen peroxide solution from BDH were used as received without further purification. A SalvisLAB Vaccucenter vacuum oven was used for annealing the PS spheres (vida infra). The platinum substrate was a 0.201 in. 10 MHz quartz crystal with a polished Pt layer (100 nm) bonded to quartz via an intermediate 10 nm Ti layer. Electrodeposition, CO stripping voltammetry, and chronoamperometric measurements were carried out on a Technobiochip Pico-balance connected to an Autolab PGSTAT 30 potentiostat/galvanostat operating under the General Purpose Electrochemical Software System (version 4.6). X-ray photoelectron spectroscopy (XPS) analysis made use of a VG ESCALAB MKII, and the narrow scan XPS spectra of Pt 4f, Ru 3p, Re 3p, and Os 3p were deconvoluted by the vendor-supplied XPSPEAK (version 4.1) software. A JEOL JSM-6700F microscope was used to obtain field-emission scanning electron microscopy (FESEM) images. The microscope was equipped with an energy-dispersive X-ray (EDX) detector thereby allowing elemental analysis to be carried out in situ. Powder X-ray diffraction (XRD) patterns were recorded by a Bruker AXS diffractometer using Cu Kα radiation at 40 kV and 40 mA.

2.2. Fabrication of Macroporous Metal Films on the Pt Quartz Crystal Substrate. The polished Pt quartz crystal substrate was ultrasonically bathed in a 3:1 (v/v) mixture of H_2SO_4 and H_2O_2 for 10 min, washed copiously with distilled water, and dried in flowing nitrogen. A colloidal solution of monodispersed PS spheres with a diameter of 433 nm was synthesized by an emulsifier-free emulsion polymerization technique.[29,30] A conventional vertical deposition method[31] was used to assemble the PS spheres on the Pt substrate into a face-centered cubic (fcc) close pack. The PS layer was then heated in a vacuum at 108.3 °C for 20 min to flatten the PS−Pt point contacts into area contacts. Ru, Re, Os, RuRe, and RuOs were deposited into the interstices of the PS array by pulse electrodeposition under the conditions shown in Table 1. The metal film thickness was controlled by the time of deposition to a height approximately equal to one-half of the PS sphere diameter. Tetrahydrofuran was then used to remove the PS spheres from the Pt substrate, leaving behind a macroporous oxophilic metal film with an orderly array of pores. The oxophilic metal film on Pt was repeatedly washed with ethanol and distilled water to remove residues of solvent and salts and was subsequently characterized by FESEM, EDX analysis, XRD, and XPS. The coverage of

(17) Wijnhoven, J. E. G. J.; Zevenhuizen, S. J. M.; Hendriks, M. A.; Vanmaekelbergh, D.; Kelly, J. J.; Vos, W. L. *Adv. Mater.* **2000**, *12*, 888.
(18) Xu, L.; Zhou, W. L.; Frommen, C.; Baughman, R. H.; Zakhidov, A. A.; Malkinski, L.; Wang, J.-Q.; Wiley, J. B. *Chem. Commun.* **2000**, 997.
(19) Bartlett, P. N.; Birkin, P. R.; Ghanem, M. A. *Chem. Commun.* **2000**, 1671.
(20) Bartlett, P. N.; Baumberg, J. J.; Birkin, P. R.; Ghanem, M. A.; Netti, M. C. *Chem. Mater.* **2002**, *14*, 2199.
(21) Zhukov, A. A.; Ghanem, M. A.; Goncharov, A. V.; de Groot, P. A. J.; El-Hallag, I. S.; Bartlett, P. N.; Boardman, R.; Fangohr, H. *J. Magn. Magn. Mater.* **2004**, *272−276*, 1621.
(22) Sumida, T.; Wada, Y.; Kitamura, T.; Yanagida, S. *Chem. Commun.* **2000**, 1613.
(23) Bartlett, P. N.; Birkin, P. R.; Ghanem, M. A.; Toh, C. S. *J. Mater. Chem.* **2001**, *11*, 849.
(24) Cassagneau, T.; Caruso, F. *Adv. Mater.* **2002**, *14*, 34.
(25) Braun, P. V.; Wiltzius, P. *Nature* **1999**, *402*, 603.
(26) Braun, P. V.; Wiltzius, P. *Adv. Mater.* **2001**, *13*, 482.
(27) Bartlett, P. N.; Dunford, T.; Ghanem, M. A. *J. Mater. Chem.* **2002**, *12*, 3130.
(28) Kavan, L.; Zukalova, M.; Kalbac, M.; Graetzel, M. *J. Electrochem. Soc.* **2004**, *151*, A1301.
(29) Cattaneo, C.; Sanchez de Pinto, M. I.; Mishima, H.; Lopez de Mishima, B. A.; Lescano, D.; Cornaglia, L. *J. Electroanal. Chem.* **1999**, *461*, 32.
(30) Okamoto, Y. *Chem. Phys. Lett.* **2005**, *405*, 79.
(31) Jiang, P.; Bertone, J. F.; Hwang, K. S.; Colvin, V. L. *Chem. Mater.* **1999**, *11*, 2132.

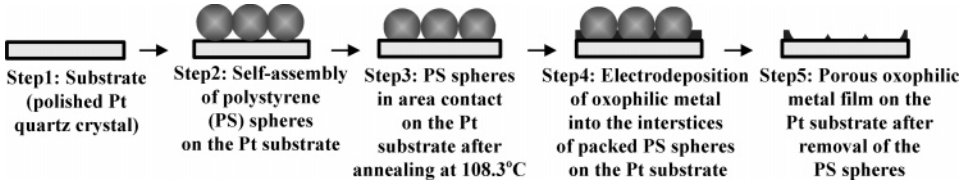

Figure 1. Schematic of preparation of porous oxophilic metal films on the Pt quartz crystal substrate with self-assembled PS spheres as the template.

oxophilic metal on the Pt quartz crystal substrate was approximately 85%.

2.3. Electrochemical Measurements. A standard three-electrode electrolysis cell was used for the electrochemical measurements. The working electrode was the Pt quartz crystal covered with the macroprous oxophilic metal film. A platinum rod and an Ag/AgCl (3 M KCl) electrode were used as the counter and the reference electrodes, respectively. All potentials were referred to the Ag/AgCl (3 M KCl) standard. Before measurements the working electrode was polarized cathodically at −0.48 V for 120 s in 0.1 M $HClO_4$ to reduce the metal surface oxides to their respective metals.[16,32] For CO stripping voltammetry the electrode was polarized at −0.14 V while the electrolyte (0.1 M $HClO_4$) was purged with 10 mol % of CO in Ar for 900 s, followed by a stream of pure Ar for another 900 s. Cyclic voltammograms were collected between −0.16 and +0.6 V for the first two scans at 20 mV s^{-1}, with the first scan starting at the adsorption potential of −0.14 V. For methanol electrooxidation an electrolyte of 0.5 M CH_3OH + 0.1 M $HClO_4$ was used. The electrolyte was deaerated by Ar for 30 min prior to chronoamperometric measurements, which were carried out at 0.4 V for 3600 s after electrode pretreatment at − 0.12 V for 120 s. All measurements were performed at room temperature of 25 °C.

3. Results and Discussion

3.1. FESEM, XRD, and XPS Characterizations. Following the scheme shown in Figure 1, homogeneous macroporous films of Ru, Os, Re RuOs, and RuRe on polished Pt quartz crystals were obtained by the pulse electrodeposition of metal(s) into the interstices of vacuum-annealed closely packed 433 nm PS spheres, followed by the solvent removal of the latter. Figure 2 shows the FESEM images of the metal films after removal of the PS spheres. The time and temperature of PS annealing were carefully controlled to give approximately the same average pore diameters (D_{pore}) in the five different films: 165.9 ± 2.1 nm for Ru, 170.4 ± 3.9 nm for Os, 161.5 ± 3.5 nm for Re, 170.9 ± 8.3 nm for co-deposited RuOs, and 160.7 ± 5.5 nm for co-deposited RuRe. For the 0.205 cm^2 Pt QCM (quartz crystal microbalance) substrate, the "uncovered" substrate areas due to Pt were 0.030 24 cm^2 for Pt−Ru, 0.0319 cm^2 for Pt−Os, 0.031 08 cm^2 for Pt−Re, 0.032 06 cm^2 for Pt−RuOs (co-deposited), and 0.028 42 cm^2 for Pt−RuRe (co-deposited). Correspondingly, the ratio of Pt on the pair sites relative to Pt on the Pt-only sites was about seven times that of the nanorods (1:1409; 1:212 for Ru, 1:218 for Os, 1:207 for Re, 1:219 for RuOs, and 1:206 for RuRe)[16]

$$\text{ratio} = \frac{\pi D_{pore}/D_{Pt}}{\pi\left(\frac{D_{pore}}{2}\right)^2/\pi\left(\frac{D_{Pt}}{2}\right)^2} = \pi\frac{D_{Pt}}{D_{pore}}$$

where D_{Pt} is the Pt atomic diameter 0.278 nm, assuming a geometrically smooth Pt surface.

The gradient in contrast in the oxophilic metal film indicating increasing film thickness radiating outward from the PS centers mirrored the geometry of the interstices formed by the flattened PS spheres. For the co-deposited bimetallics in situ EDX analyses indicated a Ru/Os ratio of 4.4:1 for the RuOs film, and a Ru/Re ratio of 4.6:1 for the RuRe film.

Figure 3 shows the XRD patterns of the Pt quartz crystal and various porous oxophilic metal films on Pt. Besides the peaks arising from the substrate corresponding to fcc platinum[16] at 2θ = 39.9° (111), 46.7° (200), 67.9° (220), 81.8° (311), and 86.1° (222), the following peaks were found for the respective deposited films: hexagonal close-pack (hcp) ruthenium (JCPDS no. 06-0663, 1999) characterized by peaks at 2θ = 44.3° (101), 58.5° (102), and 69.7° (110); hcp osmium[13] characterized by peaks at 2θ = 38.1° (100), 57.9° (102), and 69.0° (110); and tetrahedral close-pack (tcp) hydrogen rhenium oxide hydrate (JCPDS no. 80-0049, 1999) characterized by peaks at 2θ = 16.6° (101), 25.6° (112), 27.5° (004), 30.6° (200), 35.1° (121), 47.5° (116), 49.6° (125), 51.5° (132), 52.6° (224), 56.9° (008), 61.1° (323), 63.8° (400), and 66.4° (141). The presence of Re as tcp $H(ReO_4)H_2O$ instead of hcp Re in the porous Re film indicates that the as-deposited Re was easily oxidizable by water vapor and oxygen in air, as expected from a comparison of the gas-phase dissociation energies of binary oxides (Re−O, 625 kJ/mol; Os−O, 575 kJ/mol; and Ru−O, 528 kJ/mol).[5,8] The hcp peaks at 2θ = 43.8° (101), 58.0° (102), and 69.3° (110) for the porous co-deposited RuOs film were negatively shifted with respect to Ru. Because the Ru/Os ratio in the RuOs film was 4.4:1, the film was a solid solution of Os in Ru and the Bragg angle shifts were caused by the displacement of Ru atoms from their lattice positions by the larger Os atoms. For the porous co-deposited RuRe film, the XRD pattern (2θ = 43.4° (101), 57.6° (102), and 68.8° (110)) again showed a hcp structure with negative Bragg angle shifts with respect to Ru suggesting the substitution of Ru lattice positions by Re atoms, and the resulting increase in the *d* spacing (the Ru/Re ratio in RuRe film was 4.6:1).

The porous Ru, Os, Re, RuOs (co-deposited), and RuRe (co-deposited) films on Pt were also analyzed by XPS. The Pt 4f spectra of pure Pt, Ru/Pt, Os/Pt, Re/Pt, RuOs/Pt, and RuRe/Pt were all similar. Figure 4 shows a sample spectrum taken from the porous Ru film on Pt. The Pt 4f region could be deconvoluted into three pairs of doublets: Pt^0, Pt^{II}, and Pt^{IV}, respectively.[16] For each doublet, the binding energy (BE) of Pt $4f_{5/2}$ was about 3.3 eV higher than that of Pt $4f_{7/2}$. The Pt $4f_{5/2}$ BEs of Pt^0, Pt^{II}, and Pt^{IV} and their relative integrated intensities are summarized in Table 2. It is evident that Pt^0 dominated on the surface of the Pt substrate.

(32) Wu, G.; Li, L.; Xu, B. *Electrochim. Acta* **2004**, *50*, 1.

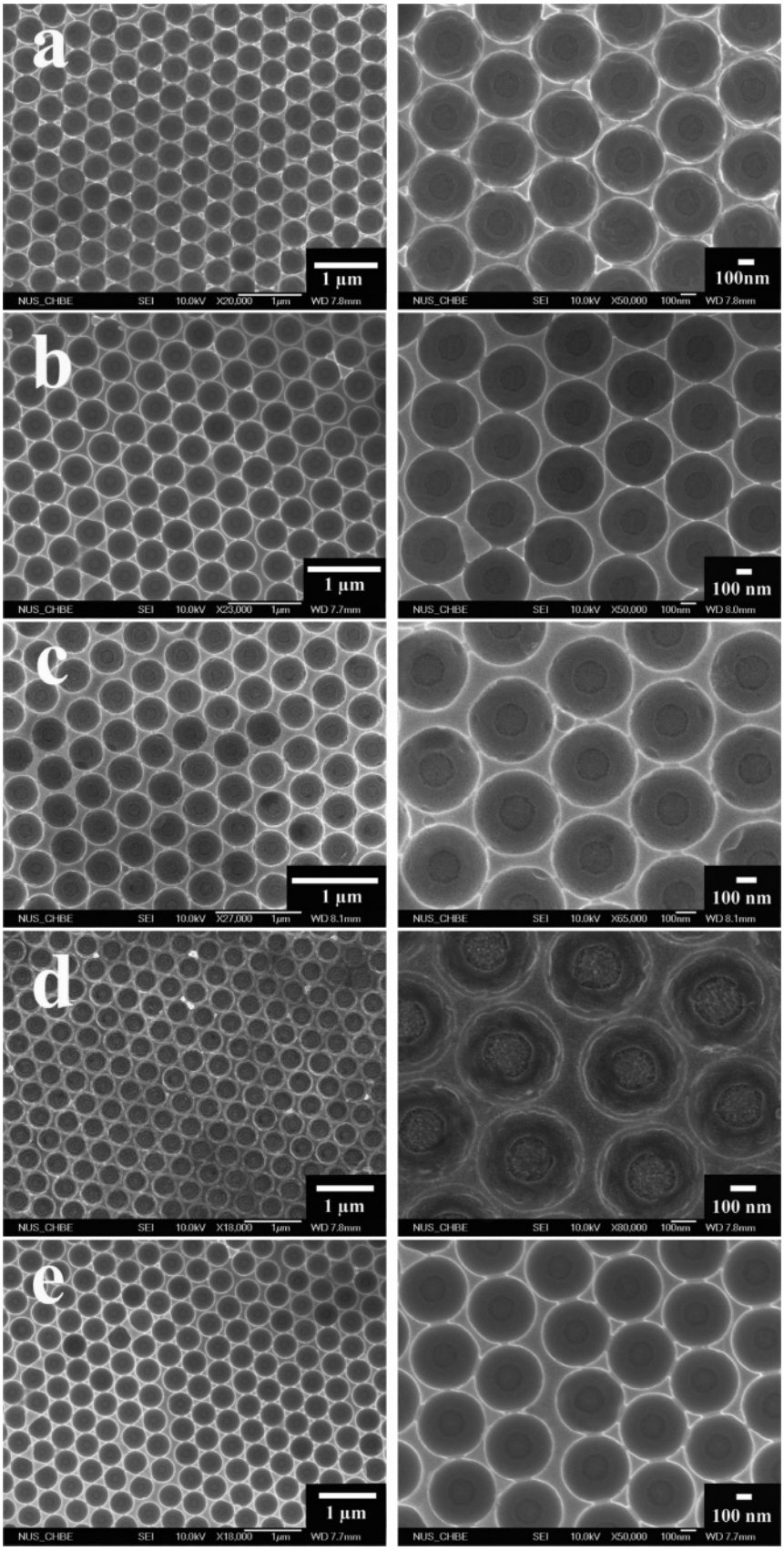

Figure 2. FESEM images of porous oxophilic metal films on polished Pt quartz crystal: (a) Ru, (b) Os, (c) Re, (d) co-deposited RuOs, and (e) co-deposited RuRe. Enlarged views of the images are shown in the right-hand column.

For the porous Ru, RuOs, and RuRe films on Pt, the overlap of the Ru $3d_{3/2}$ peak with the C 1s peak from adventitious carbon made it difficult to determine the Ru content from the Ru $3d_{3/2}$ peak, and the Ru $3p_{3/2}$ signal was used instead (Figure 5a−c). For the Ru film, the Ru $3p_{3/2}$ signal could be deconvoluted into two peaks of different intensities contributed by Ru^0 and Ru^{VI} (e.g., RuO_3), respectively.[11] For the RuOs and RuRe films, the Ru $3p_{3/2}$

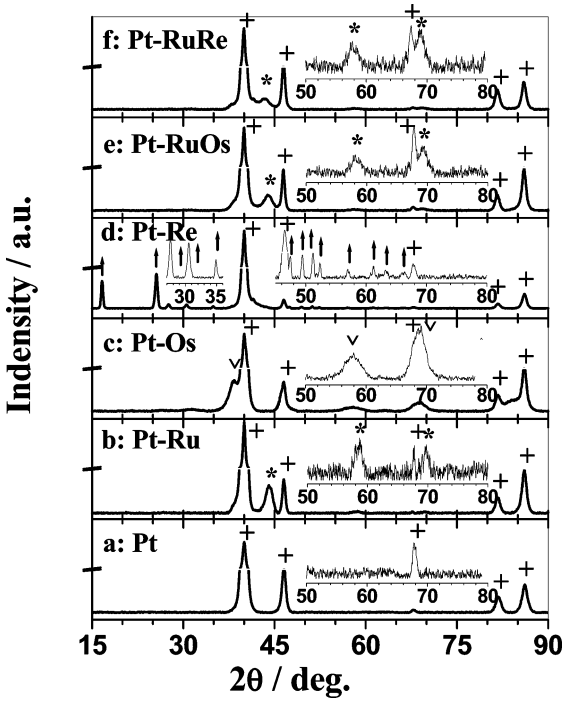

Figure 3. XRD patterns of Pt quartz crystal and various porous oxophilic metal films on the Pt quartz crystal after the removal of PS spheres. The insets are magnified views within the specified 2θ ranges. + symbols are peaks from fcc Pt; * symbols are peaks from hcp Ru; v symbols are peaks from hcp Os; and ↑ symbols are peaks from tcp $H(ReO_4)(H_2O)$.

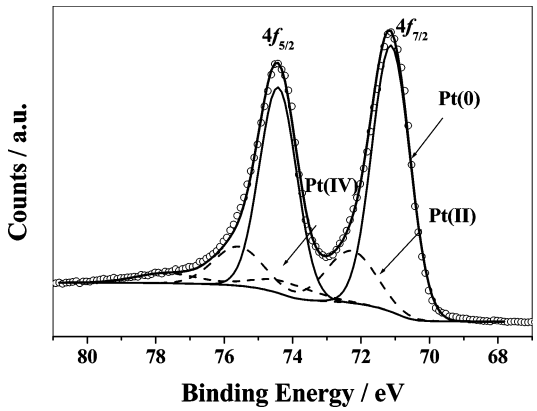

Figure 4. XPS spectra of the porous Ru film on the Pt substrate in the Pt 4f region.

signals could be deconvoluted into three peaks of different intensities attributed to Ru^0, Ru^{IV} (e.g., RuO_2), and Ru^{VI} (e.g., RuO_3).[11] When Ru is alloyed with a more oxophilic metal such as Os and Re,[5,8] the adsorbed oxygen species on Os and Re atoms may also oxidize some neighboring Ru atoms into Ru oxides. This was evident in the experimental results which showed 91.66% Ru^0 on the surface of Ru, 78.85% Ru^0 on the surface of RuOs, and 75.87% Ru^0 on the surface of RuRe. Correspondingly some higher oxidation states of Ru were detected on the surface of RuOs and RuRe films (9.98% Ru^{IV} and 11.17% Ru^{VI} on the RuOs surface and 9.18% Ru^{IV} and 14.95% Ru^{VI} on the RuRe surface compared to only 8.34% Ru^{VI} on the Ru surface). The Ru^0 and Ru^{VI} peaks for the RuRe film were also shifted to lower BEs by 0.62 and 0.86 eV, respectively, relative to Ru. When Ru (electronegativity of 2.2) is alloyed with Re, an element with a lower electronegativity (1.9), electron transfer from Re to Ru is a possibility, which may explain the observed negative shifts in the Ru BEs. The fact that the BEs of Ru^0 and Ru^{VI} for the RuOs film were somewhat higher than the corresponding values for Ru suggests a slight electron transfer from Ru to Os, even though the electronegativity of Os is about the same as that of Ru (2.2). From the integrated intensities of the deconvoluted Ru XPS signals, it is obvious that Ru^0 was the principal oxidation state on the Ru surface for all of the three Ru containing films.

For the porous Os and RuOs films on Pt, XPS (Figure 6a,b) highlighted the existence of Os^0 and OsO_2.[15] The BE difference between Os $4f_{7/2}$ and Os $4f_{5/2}$ was 2.7 eV. The BEs of Os^0 and OsO_2 for the RuOs film were lower than those for the Os film, confirming the electron transfer from Ru to Os concluded from the analysis of the Ru XPS signal. The integrated intensities of deconvoluted Os signals showed that Os^0 was the predominant Os surface species, and alloyed Os was apparently easier to oxidize in air compared to elemental Os.

Finally Figure 7a,b shows the Re 4f spectra of porous Re and RuRe films on Pt. From the known high gas-phase dissociation energy of binary Re−O compounds[5] and the aforementioned XRD pattern which shows that Re primarily existed as $H(ReO_4)H_2O$ even in the bulk, it is of no surprise to find that Re was all oxidized to Re^{VII} on the surface.[33] For the Re $4f_{5/2}$ and $4f_{7/2}$ doublet, the BE of Re $4f_{5/2}$ was about 2.43 eV higher than that of Re $4f_{7/2}$.

3.2. Electrochemical Studies. CO stripping measurements were carried out by polarizing the working electrode at the selected adsorption potential (−0.14 V) and by saturating the acidic electrolyte (0.1 M $HClO_4$) with 10% CO in Ar. After 900 s of adsorption, the electrolyte was purged of CO with pure Ar. Figure 8a,b shows the voltammograms for the first two scans of Pt and porous Os film on Pt when the potential was swept between −0.16 and +0.6 V at 20 mV s^{-1} (the first scan was started earlier, at the adsorption potential of −0.14 V). The CO stripping curves of porous Ru, RuOs, and RuRe films on Pt were similar to that of the Os film on Pt, and for clarity of presentation, only the data from their respective first forward scans are included in Figure 8b. The CO stripping curve of the porous Re film on Pt was identical to that of pure Pt because the experimental conditions had caused the complete dissolution of Re in the electrolyte. On the contrary, Re in the RuRe alloy was more resistant to electrolyte dissolution apparently because of the enhanced stability of Re in the Ru lattice. In general CO_{ad} oxidation was complete in the first scan with the second scan contributed to mostly by double-layer charging, water dissociation reaction, and metal oxidation. The CO striping curves could, therefore, be more precisely determined by subtracting the features in the second scan from those in the first scan. The resulting "background-corrected" CO stripping curves (Figure 8c) showed nearly the same CO_{ad} charge for Pt, Pt−Ru, Pt−Os, Pt−RuOs, and Pt−RuRe, even though 85% of the Pt surface was covered by the oxophilic metal(s). This suggests that CO adsorption occurred not only on the Pt surface but also on the oxophilic metals, as has been previously known (Ru,[34] Os,[35] and Re[36]).

(33) Cimino, A.; De Angelis, B. A.; Gazzoli, D.; Valigi, M. *Z. Anorg. Allg. Chem.* **1980**, *460*, 86.

Table 2. Chemical States, BEs, and Ratios of Integrated Intensities (AR) of Porous Ru, Os, Re, RuOs, and RuRe Films on Pt Quartz Crystal

		Pt $4f_{7/2}$			Ru $3p_{3/2}$			Os $4f_{7/2}$		Re $4f_{7/2}$
samples		Pt^0	Pt^{II}	Pt^{IV}	Ru^0	Ru^{IV}	Ru^{VI}	Os	OsO_2	Re^{VII}
Pt−Ru	BE (eV)	71.08	72.32	74.34	461.82		465.14			
	AR (%)	74.89	19.06	6.05	91.66		8.34			
Pt−Os	BE (eV)	71.06	72.31	74.31				50.40	52.24	
	AR (%)	74.22	19.15	6.63				73.24	26.76	
Pt−Re	BE (eV)	71.07	72.39	74.33						46.29
	AR (%)	74.90	19.09	6.01						100
Pt−RuOs	BE (eV)	71.08	72.33	74.31	461.89	463.53	465.17	49.37	50.92	
	AR (%)	74.88	19.12	6.00	78.85	9.98	11.17	62.77	37.23	
Pt−RuRe	BE (eV)	71.07	72.38	74.29	461.20	462.75	464.28			46.55
	AR (%)	74.37	19.22	6.41	75.87	9.18	14.95			100

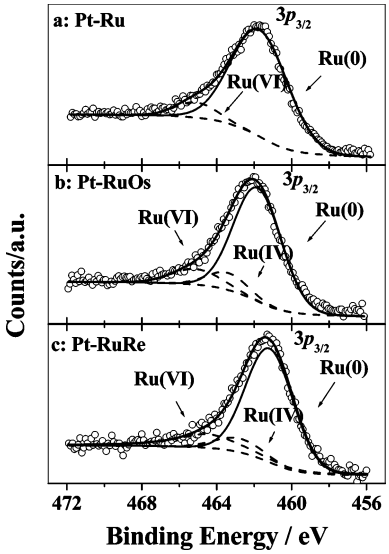

Figure 5. XPS spectra in the Ru 3p region for porous (a) Ru, (b) RuOs, and (c) RuRe films on Pt.

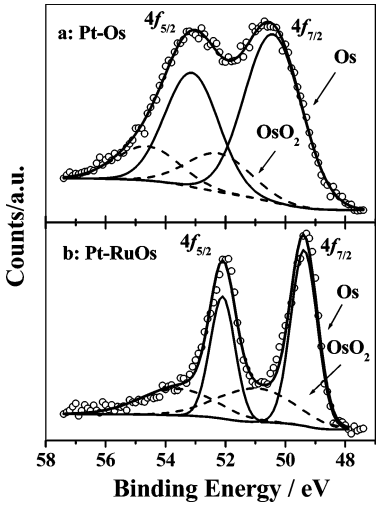

Figure 6. XPS spectra in the Os 4f region for porous (a) Os and (b) RuOs films on Pt.

The kinetics of CO_{ad} oxidation on catalytic metals is determined by four factors: water dissociation on the metal surface to form $-OH_{ad}$; the strength of the metal$-OH_{ad}$ bond; the strength of the metal$-CO_{ad}$ bond; and the surface reaction

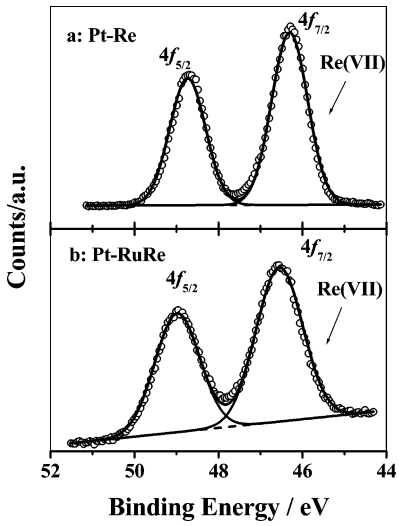

Figure 7. XPS spectra in the Re 4f region for porous (a) Re and (b) RuRe films on Pt.

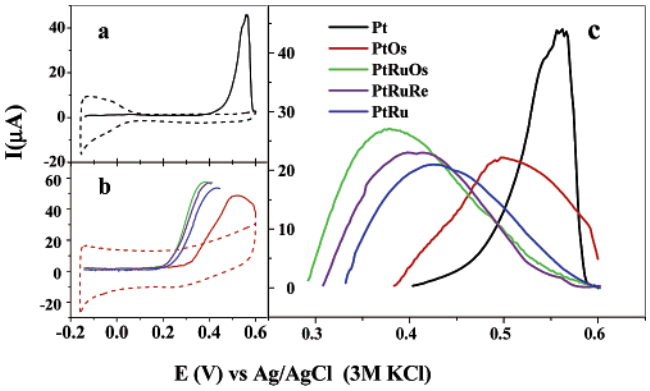

Figure 8. (a) First two scans of CO stripping voltammograms for Pt quartz crystal substrate in 0.1 M $HClO_4$; (b) cyclic voltammograms of CO stripping for porous Os film on Pt (red). Solid line: first scan. Dashed line: second scan. (c) Oxidation of pre-adsorbed CO on Pt quartz crystal substrate (black), porous Ru on Pt (blue), Os on Pt (red), RuOs on Pt (green), and RuRe on Pt (purple) after background correction (see text). Electrolyte: 0.1 M $HClO_4$. Scan range, −0.16 V to +0.6 V versus Ag/AgCl (3 M KCl); scan rate, 20 mV s^{-1}; temperature, 25 °C; electrolyte, 0.1 M $HClO_4$. Also included are the first forward scans of the CO stripping voltammograms for porous Ru−Pt (blue), RuOs−Pt (green), and RuRe−Pt (purple).

between CO_{ad} and $-OH_{ad}$ leading to CO_2. According to a previous calculation,[37] the ability to dissociate water is ranked in the following order: Ru > Os > Pt. The BEs of $-OH_{ad}$ on Pt, Ru, and Os are 40.79, 49.30, and 51.35 kcal/mol, respectively, indicating that it is easier to remove $-OH_{ad}$

(34) Gasteiger, H. A.; Markovic, N. M.; Ross, P. N. *J. Phys. Chem.* **1995**, *99*, 8290.
(35) Orozco, G.; Gutierrez, C. *J. Electroanal. Chem.* **2000**, *484*, 64.
(36) Grgur, B. N.; Markovic, N. M.; Ross, P. N. *Electrochim. Acta* **1998**, *43*, 3631.
(37) Kua, J.; Goddard, W. A. *J. Am. Chem. Soc.* **1999**, *121*, 10928.

from the Pt surface than from the surface of Ru or Os (in that order). The BEs of CO_{ad} on Pt, Ru, and Os are 41.88, 26.25, and 34.53 kcal/mol, and, hence, the ease of removal of CO_{ad} on the three metals should follow the order Ru > Os > Pt. The surface reaction between $-OH_{ad}$ and CO_{ad} should proceed equally efficiently on all three metals after OH_{ad} and CO_{ad} are sufficiently weakened at their binding sites. On the basis of these arguments CO_{ad} oxidation should be more facile on Ru than on Os because Ru promotes water dissociation, and the binding of $-OH_{ad}$ and CO_{ad} on Ru is also weaker. While OH_{ad} is only weakly held by the Pt surface, Pt is handicapped by the difficulty in water dissociation and by the strength of the $Pt-CO_{ad}$ bond. The onset potentials for CO removal in Figure 8c (~0.33 V for Ru, ~0.38 V for Os, and ~0.40 V for Pt) basically confirm the difficulty of CO_{ad} oxidation on Pt.

Because water dissociation and $-OH_{ad}$ removal are both more facile on Ru than on Os, CO_{ad} oxidation should be more efficient on the Ru−Pt pair sites than on the Os−Pt pair sites. CO_{ad} on Pt is removed by reaction with OH_{ad} on a neighboring oxophilic metal site. Below the potential for water dissociation on Pt, the reacted CO_{ad} is replenished by the surface diffusion of CO_{ad} from the remote Pt-only sites to the pair sites. The mobility of CO_{ad} is good on large Pt particles[38] and on a smooth electrode surface[39] such as the Pt QCM substrate. In the event of limited CO_{ad} mobility (e.g., in a sulfate containing electrolyte[40]), rapid OH_{ad} spillover from the oxophilic metal to the pair sites is a possibility.[41] The OH_{ad} spillover effect would not be a key consideration here because a sulfate-free electrolyte was used. On the basis of these considerations the CO oxidation peak potential for Pt covered with porous Ru would be lower than that for Pt covered with porous Os, which in turn would be lower than that for pure Pt. The inference is supported by experimental measurements shown in Figure 8c: peak potentials of 0.43 V for Pt−Ru and 0.52 V for Pt−Os. For pure Pt this would have to occur at the potential for water dissociation which is 0.56 V,[34] resulting in a very steep CO stripping curve.

When Ru was alloyed with the more oxophilic metals of Os and Re, the onset potentials shifted negatively by 0.04 and 0.02 V respectively. This indicates that alloying has weakened the adsorption strengths of $-OH_{ad}$ or CO_{ad}, although not significantly. The peak potentials for CO oxidation were shifted negatively by ~0.05 and ~0.03 V for the porous RuOs and RuRe films, respectively. The percentages of Ru as RuO_x on the RuOs and RuRe surfaces were 21.15% and 24.13%. The Os sites in the RuOs surface also contained 37.23% of OsO_2 (and 62.77% of Os), whereas Re in the surface of RuRe was 100% of Re_2O_7. XPS results have shown that the BE of $-OH_{ad}$ was weaker on RuOs, and, hence, RuOs was more adept at supplying OH_{ad} to a neighboring Pt site for collaborative CO_{ad} removal, rationalizing the lower peak potential for CO oxidation on the Pt−RuOs film.

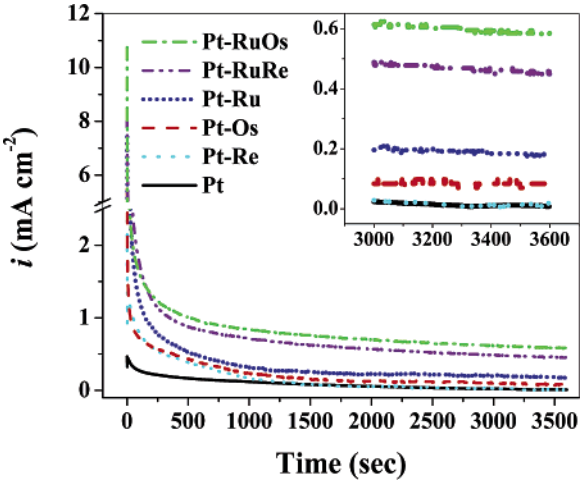

Figure 9. Current density−time plots of the Pt substrate and porous Ru, Os, Re, RuOs, and RuRe films on Pt in Ar-purged 0.1 M $HClO_4$ and 0.5 M CH_3OH polarized at a constant potential of 0.4 V versus Ag/AgCl (3 M KCl) at 25 °C. The current density is normalized by the uncovered Pt surface area in each sample.

Current density−time curves measured at a fixed potential were used to project the long-term performance of the various pair sites in the electrooxidation of methanol at room temperature. Figure 9 shows current densities measured at +0.4 V versus Ag/AgCl (3 M KCl) for a period of 3600 s in an Ar-purged solution of 0.5 M CH_3OH in 0.1 M $HClO_4$. The electrode was conditioned at −0.12 V for 120 s prior to the measurements to ensure that there was no methanol adsorption on the catalyst surface. The high initial current was contributed to by double-layer charging[42] and by the large number of active sites initially available for methanol activation. Current density declined sharply within the first few seconds of potential imposition[43] as the Pt sites were progressively deactivated by the CO-like intermediates formed in the dissociative chemisorption of methanol. It was followed by a hyperbolic decay[42] before a pseudo-steady state was reached in approximately 1500 s. The porous RuOs film on Pt exhibited the highest oxidation current density at 3600 s (0.58 mA cm^{-2}), followed by porous RuRe film on Pt (0.45 mA cm^{-2}), porous Ru film on the Pt substrate (0.17 mA cm^{-2}), and porous Os film on Pt (0.08 mA cm^{-2}). Because of the electrolyte dissolution of Re, the porous Re film on Pt behaved identically to the Pt substrate, producing the same lowest oxidation current density (0.008 mA cm^{-2}). Because Pt sites away from the Pt−oxophilic metal interface were severely deactivated as a result of the lack of a renewal mechanism, their contribution to the measured current densities was negligible, and this had been confirmed by measurements using a pure Pt substrate. Control experiments using Ru, Os, Re, RuOs, and RuRe films without Pt also showed no residual activity on methanol electrooxidation under the same experimental conditions. Hence, the pseudo-steady state activities in Figure 9 are characteristics of the ability of the pair sites in turning over the tenacious CO-like reaction intermediates. In this regard the Pt−RuOs

(38) Maillard, F.; Eikerling, M.; Cherstiouk, O. V.; Schreier, S.; Savinova, E.; Stimming, U. *Faraday Discuss.* **2004**, 357.
(39) Lu, G. Q.; Waszczuk, P.; Wieckowski, A. *J. Electroanal. Chem.* **2002**, *532*, 49.
(40) Davies, J. C.; Hayden, B. E.; Pegg, D. J.; Rendall, M. E. *Surf. Sci.* **2002**, *496*, 110.
(41) Desai, S.; Neurock, M. *Electrochim. Acta* **2003**, *48*, 3759.
(42) Chu, D.; Gilman, S. *J. Electrochem. Soc.* **1996**, *143*, 1685.
(43) Jiang, L.; Zhou, Z.; Li, W.; Zhou, W.; Song, S.; Li, H.; Sun, G.; Xin, Q. *Energy Fuels* **2004**, *18*, 866.

pair sites had shown the most sustainable activity, followed by the Pt−RuRe, Pt−Ru, and Pt−Os pair sites, in exactly the same order as that measured by CO stripping voltammetry.

According to the theory of bifunctional catalysis, methanol dissociation occurs on the Pt sites, and water dissociation occurs on the oxophilic metal sites. Because there was no clear indication of an electronic effect by XPS measurements, it is assumed that the BE of CO on Pt would not be affected by neighboring atoms of the electrodeposited oxophilic metal. Consequently the difference in the CO removal rate for the various pair sites (Pt−Ru, Pt−Os, Pt−RuOs, and Pt−RuRe) must be traceable to the ability of the pair sites in providing chemically labile OH_{ads}. For monometallic oxophilic metals, the effectiveness of Ru (relative to Os, as Re is unstable in acidic electrolytes) can be understood on the basis of the $M-OH_{ad}$ bond strength considerations alone. For bimetallic oxophilic metal combinations, the resilient activity of the Pt−RuOs site relative to Pt−RuRe and Pt−Ru can likewise be rationalized in terms of the weakening of the BE of OH_{ad} due to alloying. XPS results have shown that the weakening effect was the strongest in the RuOs system.

4. Conclusions

The use of porous oxophilic metal films on Pt with distinct Pt−oxophilic metal interfaces removes many of the uncertainties in attributing the measured activity difference to the intrinsic chemistry of the various pair sites. Unlike conventionally prepared alloy catalysts where the control of particle geometry and composition is a perennial problem, the porous metal films prepared here have the same pore diameter, the same pore layout, and an increased number of pair sites compared to multisegment nanorods. From both CO stripping voltammetry and chronoamperometric measurements in acidic electrolytes, the Pt−RuOs pair sites showed the best CO tolerance and consequently the most sustainable catalytic activity in methanol oxidation, followed by the Pt−RuRe pair sites, the Pt−Ru pair sites, and the Pt−Os pair sites. On the other hand the Pt−Re pair sites were ineffective because of the selective etching of Re by the electrolyte.

Acknowledgment. F.L. acknowledges the National University of Singapore for her research scholarship.

CM0606023